




Cite this: *Chem. Sci.*, 2024, 15, 9281

All publication charges for this article have been paid for by the Royal Society of Chemistry

Received 11th April 2024  
Accepted 16th May 2024  
DOI: 10.1039/d4sc02384f  
rsc.li/chemical-science

# Self-assembled molecular hybrids comprising lacunary polyoxometalates and multidentate imidazole ligands†

Haoran Sun, Atsuhiko Jimbo, Chifeng Li, Kentaro Yonesato,  Kazuya Yamaguchi   
and Kosuke Suzuki \*

Self-assembly *via* coordination bonding facilitates the creation of diverse inorganic–organic molecular hybrids with distinct structures and properties. Recent advances in this field have been driven by the versatility of organic ligands and inorganic units. Lacunary polyoxometalates are a class of well-defined metal-oxide clusters with a customizable number of reactive sites and bond directions, which make them promising inorganic units for self-assembled molecular hybrids. Herein, we report a novel synthesis method for self-assembled molecular hybrids utilizing the reversible coordination of multidentate imidazole ligands to the vacant sites of lacunary polyoxometalates. We synthesized self-assembled molecular hybrids including monomer, dimers, and tetramer, demonstrating the potential of our method for constructing intricate hybrids with tailored properties and functionalities.

## Introduction

Self-assembly *via* coordination bonding is a powerful approach for constructing various inorganic–organic molecular hybrids with interesting applications such as catalysis, reactivity control, molecular recognition, and separation.<sup>1</sup> Recent remarkable advances in this field have been enabled by the diversity and design possibilities of both organic ligands and inorganic units. Polyoxometalates (POMs) are a class of structurally well-defined inorganic metal-oxide clusters, where metals are typically in high oxidation states such as Mo<sup>6+</sup>, W<sup>6+</sup>, and V<sup>5+</sup>.<sup>2</sup> Their structures and constituent elements can be tailored to facilitate the modification of their chemical and physical properties for various applications, such as in catalysis, photocatalysis, sensors, batteries, and energy conversion.<sup>2</sup> Integrating organic ligands into POM systems enables further control over their stabilities, structures, and functionalities.<sup>3,4</sup> In particular, lacunary POMs, where one or more [MO<sub>x</sub>] units are removed from the plenary structure, possess vacant reactive sites for metal atoms or organic ligands.<sup>2,5</sup> Moreover, the number of reactive sites and bond directions can be tailored depending on the lacunary structure; therefore, these lacunary POMs are promising inorganic units for constructing coordination-driven inorganic–organic molecular hybrids.

Various types of organic ligands such as phosphates, amines, silanols, and alcohols have been used for constructing POM–organic hybrids *via* coordination with the vacant sites of lacunary POMs<sup>3,6</sup> or additionally incorporated metal sites at these vacant sites.<sup>7</sup>

Recently, our research group reported that pyridine-based ligands are effective for constructing POM–organic hybrids *via* reversible coordination bonds between pyridine and the vacant sites of lacunary POMs.<sup>8</sup> Three pyridine molecules can coordinate with the Mo atoms at the vacant sites of a trivacant lacunary Keggin-type phosphomolybdate (TBA<sub>3</sub>H<sub>6</sub>[A- $\alpha$ -PMo<sub>9</sub>O<sub>34</sub>], TBA = tetra-*n*-butylammonium) to form TBA<sub>3</sub>[A- $\alpha$ -PMo<sub>9</sub>O<sub>31</sub>(-pyridine)<sub>3</sub>]. Moreover, we found that this pyridine-coordinated hybrid can be reacted with multidentate pyridine-based ligands in organic solvents to synthesize more complex molecular hybrids *via* ligand exchange reactions.<sup>8</sup>

We hypothesized that imidazole is a promising ligand to expand this approach because it has a stronger coordination ability with metal ions compared with pyridine and its five-membered ring structure offers coordination directions that differ from the six-membered ring structure of pyridine-based ligands.<sup>9</sup> To date, various imidazole-based metal–organic structures such as cages and capsules have been synthesized using metal ions and imidazole ligands as building units.<sup>10</sup> Although several hybrids of POMs and imidazole ligands synthesized *via* hydrogen bonding and electronic interaction as well as coordination to the substituted metals in POMs have been reported,<sup>11</sup> a system directly coordinating imidazole to lacunary POMs has not yet been reported.

Herein, for the first time, we present a synthesis method for fabricating self-assembled molecular hybrids comprising

Department of Applied Chemistry, School of Engineering, The University of Tokyo, 7-3-1 Hongo, Bunkyo-ku, Tokyo 113-8656, Japan. E-mail: ksuzuki@appchem.t.u-tokyo.ac.jp

† Electronic supplementary information (ESI) available: Experimental details, Fig. S1–S7, Table S1. CCDC 2345494–2345497. For ESI and crystallographic data in CIF or other electronic format see DOI: <https://doi.org/10.1039/d4sc02384f>

lacunary POMs and multidentate imidazole ligands. By reacting a pyridine-coordinated trivacant lacunary phosphomolybdate  $\text{TBA}_3[\text{A-}\alpha\text{-PMo}_9\text{O}_{31}(\text{pyridine})_3]$  with four types of multidentate imidazole ligands in organic solvents, we successfully synthesized a series of self-assembled molecular POM–organic hybrids: a capped monomer **I**, pillared dimer **II**, sandwich-like dimer **III**, and tetrahedron tetramer **IV** through the direct coordination of imidazole ligands to lacunary POMs (Fig. 1).

## Results and discussion

To synthesize **I**, 1,3,5-tris[(1*H*-imidazol-1-yl)methyl]benzene (**L1**), which possesses three imidazole groups on a benzene ring through flexible methylene groups, was used as a ligand and reacted with  $\text{TBA}_3[\text{A-}\alpha\text{-PMo}_9\text{O}_{31}(\text{pyridine})_3]$  in acetonitrile at 80 °C for 10 min (**L1**:  $\text{TBA}_3[\text{A-}\alpha\text{-PMo}_9\text{O}_{31}(\text{pyridine})_3]$  = 2 : 1). This was followed by recrystallization in a mixed solvent of 1,2-dichloroethane and diethyl ether, which yielded single crystals of **I**. X-ray crystallographic analysis revealed that the anion part of **I** adopted a capped monomer structure comprising one  $[\alpha\text{-PMo}_9]$  unit and one **L1** ligand, wherein three imidazole groups of **L1** coordinated to three Mo atoms at the vacant site of the  $[\alpha\text{-PMo}_9]$  unit (Fig. 2a, Table S1†). The electrospray ionization (ESI) mass spectrum of **I** in acetonitrile exhibited sets of signals at  $m/z$

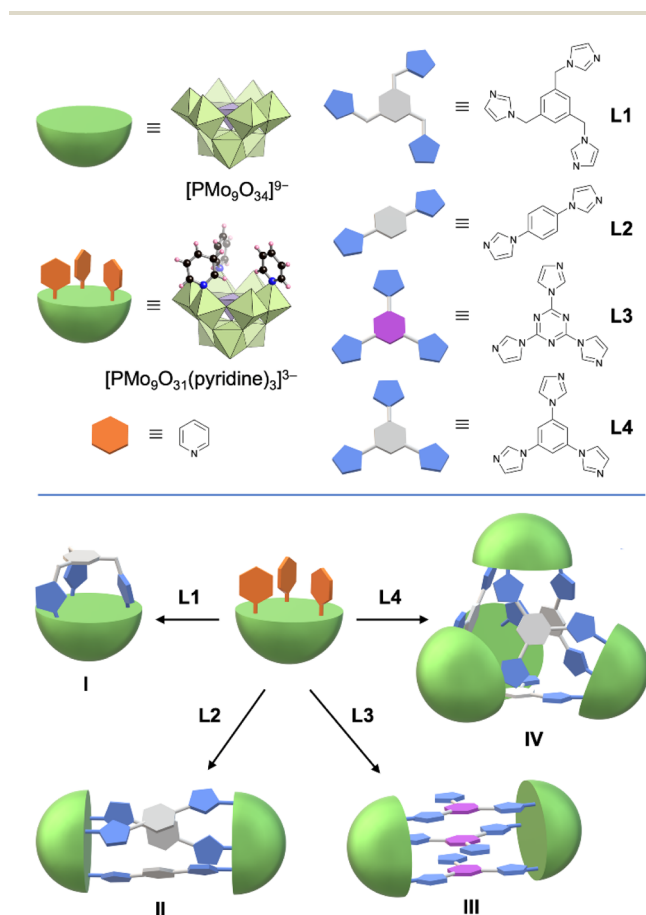


Fig. 1 Self-assembly of molecular hybrids **I**, **II**, **III**, and **IV** using multidentate imidazole ligands and pyridine-coordinated trivacant lacunary phosphomolybdate.

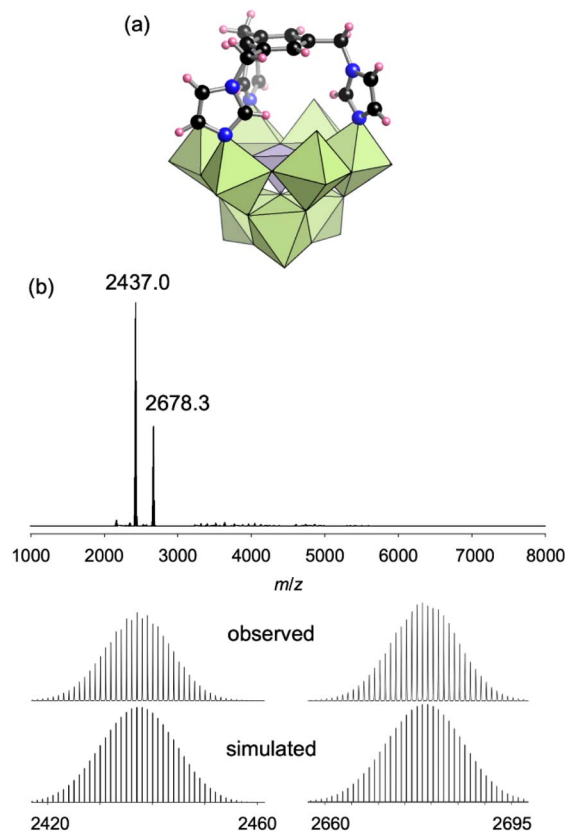


Fig. 2 (a) Crystal structure of the anion part of **I**. Light-green and light-purple polyhedra represent  $[\text{MoO}_6]$  and  $[\text{PO}_4]$ , respectively. Blue, black, and pink spheres represent N, C, and H atoms, respectively. (b) ESI mass spectrum of **I** in acetonitrile. Inset: enlarged spectra and simulated patterns for  $m/z$  2437.0 ( $[\text{TBA}_3\text{H}(\text{PMo}_9\text{O}_{31})(\text{L1})]^+$ ) and 2678.3 ( $[\text{TBA}_4(\text{PMo}_9\text{O}_{31})(\text{L1})]^+$ ).

$z$  2437.0 and 2678.3, which were attributed to  $[\text{TBA}_3\text{H}(\text{PMo}_9\text{O}_{31})(\text{L1})]^+$  and  $[\text{TBA}_4(\text{PMo}_9\text{O}_{31})(\text{L1})]^+$ , respectively (Fig. 2b). The  $^{31}\text{P}$  nuclear magnetic resonance (NMR) spectrum of **I** in acetonitrile- $d_3$  ( $\text{CD}_3\text{CN}$ ) exhibited a signal at  $-2.06$  ppm (Fig. S1a†), which was observed up-field compared with  $\text{TBA}_3[\text{A-}\alpha\text{-PMo}_9\text{O}_{31}(\text{pyridine})_3]$  ( $-0.68$  ppm).<sup>8a</sup> The  $^1\text{H}$  NMR spectrum of **I** in  $\text{CD}_3\text{CN}$  showed the splitting of the signals of the methylene H atoms in the ligand at 5.11 ppm ( $d, J = 13.5$  Hz) and 4.88 ppm ( $d, J = 13.5$  Hz), which can be ascribed to the geminal H–H spin-spin coupling on the same methylene C atom (Fig. S1b†). This observation of  $^1\text{H}$  NMR spectrum agrees with the rigid structure of **I**, where two H atoms in a methylene group exist in different chemical environments. We also confirmed that the  $^{31}\text{P}$  NMR spectrum remained almost unchanged after 3 days, demonstrating the stability of **I** in the solvent (Fig. S1c†). Based on these results as well as elemental analysis and thermogravimetry differential thermal analysis (TG-DTA) results (Fig. S2a†), the formula of **I** was determined to be  $\text{TBA}_3[\text{A-}\alpha\text{-PMo}_9\text{O}_{31}(\text{L1})](\text{C}_2\text{H}_4\text{Cl}_2)_2$ .

To construct oligomeric hybrid structures, we investigated the use of rigid multidentate ligands.  $\text{TBA}_3[\text{A-}\alpha\text{-PMo}_9\text{O}_{31}(\text{pyridine})_3]$  was reacted with 1,4-di(1*H*-imidazol-1-yl)benzene (**L2**), which is a linear ligand possessing two imidazole

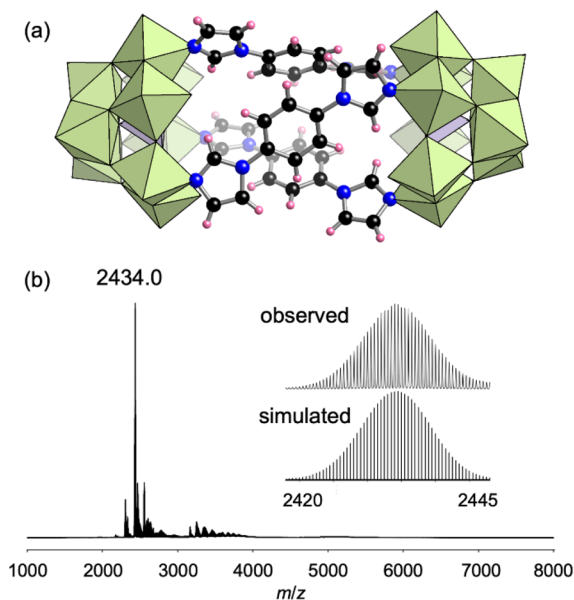


Fig. 3 (a) Crystal structure of the anion part of **II**. (b) ESI mass spectrum of **II** in acetonitrile. (Inset): enlarged spectrum and simulated pattern for  $m/z$  2434.0 ( $[\text{TBA}_6\text{H}_2(\text{PMo}_9\text{O}_{31})_2(\text{L}_2)_3]^{2+}$ ).

groups, in 3 : 1 ratio in acetonitrile at 50 °C for 10 min. By recrystallization of the crude product in 1,2-dichloroethane, single crystals of **II** suitable for X-ray crystallographic analysis were obtained. The anion part of **II** had a pillared dimer structure where two  $[\text{PMo}_9]$  units were bridged by three **L2** ligands (Fig. 3a, Table S1†). Some of the  $[\alpha\text{-PMo}_9]$  units were transformed into  $[\beta\text{-PMo}_9]$  units *via* rotation of the  $[\text{Mo}_3\text{O}_{13}]$  unit underneath by approximately 60° from the original orientation (Fig. S3†). X-ray crystallographic analysis results showed that the ratio of  $[\alpha\text{-PMo}_9]$  and  $[\beta\text{-PMo}_9]$  was 1 : 0.07. The  $^{31}\text{P}$  NMR spectrum of **II** in  $\text{CD}_3\text{CN}$  exhibited two signals at  $-1.34$  and  $-0.01$  ppm with a signal integral ratio of 1 : 0.09, which were attributed to the  $[\alpha\text{-PMo}_9]$  and  $[\beta\text{-PMo}_9]$  isomers, respectively (Fig. S4†). The ESI mass spectrum of **II** in acetonitrile exhibited a set of signals at  $m/z = 2434.0$ , which was assignable to  $[\text{TBA}_6\text{H}_2(\text{PMo}_9\text{O}_{31})_2(\text{L}_2)_3]^{2+}$  (Fig. 3b). These NMR and ESI mass spectra showed that **II** maintained its structure in the solvent. The  $^{31}\text{P}$  NMR spectrum of **II** in  $\text{CD}_3\text{CN}$  after 3 days showed only two signals at  $-1.34$  and  $-0.01$  ppm, but the integral ratio of these signals changed from 1 : 0.09 to 1 : 0.27 (Fig. S4c†). This result showed that although the ratio of  $[\alpha\text{-PMo}_9]$  and  $[\beta\text{-PMo}_9]$  in **II** changes after several days, the structure of **II** is stable and kept in the solvent. Based on these results as well as the elemental analysis and TG-DTA results (Fig. S2b†), the formula of **II** was determined to be  $\text{TBA}_{5.7}\text{H}_{0.3}[(\text{PMo}_9\text{O}_{31})_2(\text{L}_2)_3](\text{C}_2\text{H}_4\text{Cl}_2)$ .

The structure of **II** is similar to that of our previously reported hybrid dimer comprising three 4,4'-bipyridine ligands (**L5**) and two  $[\text{PMo}_9]$  units ( $[(\text{A-}\alpha\text{-PMo}_9\text{O}_{31})_2(\text{L}_5)_3]^{6-}$ ) (Fig. 4).<sup>8a</sup> Changing the pyridine-based ligand to the imidazole-based ligand shortened the Mo–N bond lengths in **II** (2.26 Å on average, Mo–imidazole coordination bonds) compared with

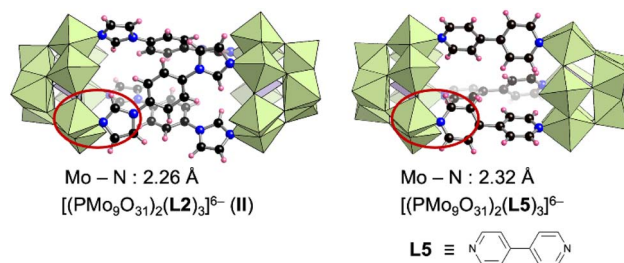


Fig. 4 Structures of  $[(\text{PMo}_9\text{O}_{31})_2(\text{L}_2)_3]^{6-}$  (**II**) and  $[(\text{PMo}_9\text{O}_{31})_2(\text{L}_5)_3]^{6-}$  and their average Mo–N bond lengths.<sup>8a</sup>

those in  $[(\text{A-}\alpha\text{-PMo}_9\text{O}_{31})_2(\text{L}_5)_3]^{6-}$  (2.32 Å on average, Mo–pyridine coordination bonds) (Fig. 4). Although only  $[\alpha\text{-PMo}_9]$  units were observed in  $[(\text{A-}\alpha\text{-PMo}_9\text{O}_{31})_2(\text{L}_5)_3]^{6-}$ , isomerized  $[\beta\text{-PMo}_9]$  units were also observed in **II**. To investigate the formation of these imidazole- and pyridine-based hybrids as well as the isomerization of  $[\alpha\text{-PMo}_9]$  to  $[\beta\text{-PMo}_9]$  units, we performed density functional theory calculations for these reactions. The standard Gibbs energy of the reaction  $2[\text{A-}\alpha\text{-PMo}_9\text{O}_{31}(\text{pyridine})_3]^{3-} + 3\text{L}_2 \rightarrow [(\text{A-}\alpha\text{-PMo}_9\text{O}_{31})_2(\text{L}_2)_3]^{6-}$  (**II**) + 3pyridine was  $-69.2$  kJ mol<sup>-1</sup>, while that for the reaction  $2[\text{A-}\alpha\text{-PMo}_9\text{O}_{31}(\text{pyridine})_3]^{3-} + 3\text{L}_5 \rightarrow [(\text{A-}\alpha\text{-PMo}_9\text{O}_{31})_2(\text{L}_5)_3]^{6-}$  + 3pyridine was  $-23.2$  kJ mol<sup>-1</sup>. These results indicate that the formation of **II** was considerably more favorable than that of  $[(\text{A-}\alpha\text{-PMo}_9\text{O}_{31})_2(\text{L}_5)_3]^{6-}$ , which is likely owing to the stronger coordination of imidazole ligands to Mo atoms when compared with pyridine ligands. In addition, we investigated the isomerization from  $[\alpha\text{-PMo}_9]$  to  $[\beta\text{-PMo}_9]$  units in the aforementioned hybrids. The standard Gibbs energies for isomerization from  $[\alpha\text{-PMo}_9]$  to  $[\beta\text{-PMo}_9]$  units in  $[(\text{A-}\alpha\text{-PMo}_9\text{O}_{31})_2(\text{L}_5)_3]^{6-}$  and **II** were 15.58 and 0.38 kJ mol<sup>-1</sup>, respectively. These results support the partial isomerization of  $[\beta\text{-PMo}_9]$  in the imidazole-based **II**.

To construct a more complex structure, we next utilized 2,4,6-(1*H*-imidazol-yl)-1,3,5-triazine (**L3**), which possesses three imidazole groups at the 1,3,5-positions of the triazine ring, as a ligand. Reacting  $\text{TBA}_3[\text{A-}\alpha\text{-PMo}_9\text{O}_{31}(\text{pyridine})_3]$  and **L3** in 2 : 1 ratio in acetonitrile at room temperature ( $\sim 25$  °C) for 30 min followed by pouring the solution into an excess amount of diethyl ether obtained **III** as a crude powder. Recrystallization of the crude product in 1,2-dichloroethane obtained single crystals of **III** suitable for X-ray crystallographic analysis, which revealed that the anion part of **III** comprised two  $[\text{PMo}_9]$  units and three **L3** ligands lying in parallel (Fig. 5a, Table S1†). For each **L3** ligand, two of three imidazole units coordinated to Mo atoms, and the other imidazole unit remained unreacted. All  $[\text{PMo}_9]$  units in the crystalline product of **III** were  $[\beta\text{-PMo}_9]$  units. The  $^{31}\text{P}$  NMR spectrum of **III** in  $\text{CD}_3\text{CN}$  exhibited a signal at 0.36 ppm, which was attributed to the  $[\beta\text{-PMo}_9]$  isomer (Fig. S5a†). The ESI mass spectrum of **III** in acetonitrile exhibited a set of signals at  $m/z$  2537.9, 2658.5, and 2779.1, which could be assigned to  $[\text{TBA}_6\text{H}_2(\text{PMo}_9\text{O}_{31})_2(\text{L}_3)_3]^{2+}$ ,  $[\text{TBA}_7\text{H}(\text{PMo}_9\text{O}_{31})_2(\text{L}_3)_3]^{2+}$ , and  $[\text{TBA}_8(\text{PMo}_9\text{O}_{31})_2(\text{L}_3)_3]^{2+}$ , respectively (Fig. 5b). Based on these results as well as elemental analysis, TG-DTA, and  $^{31}\text{P}$  NMR results (Fig. S2c and S5a†), the formula of **III** was determined as  $\text{TBA}_6[(\text{PMo}_9\text{O}_{31})_2(\text{L}_3)_3](\text{C}_2\text{H}_4\text{Cl}_2)_2$ .



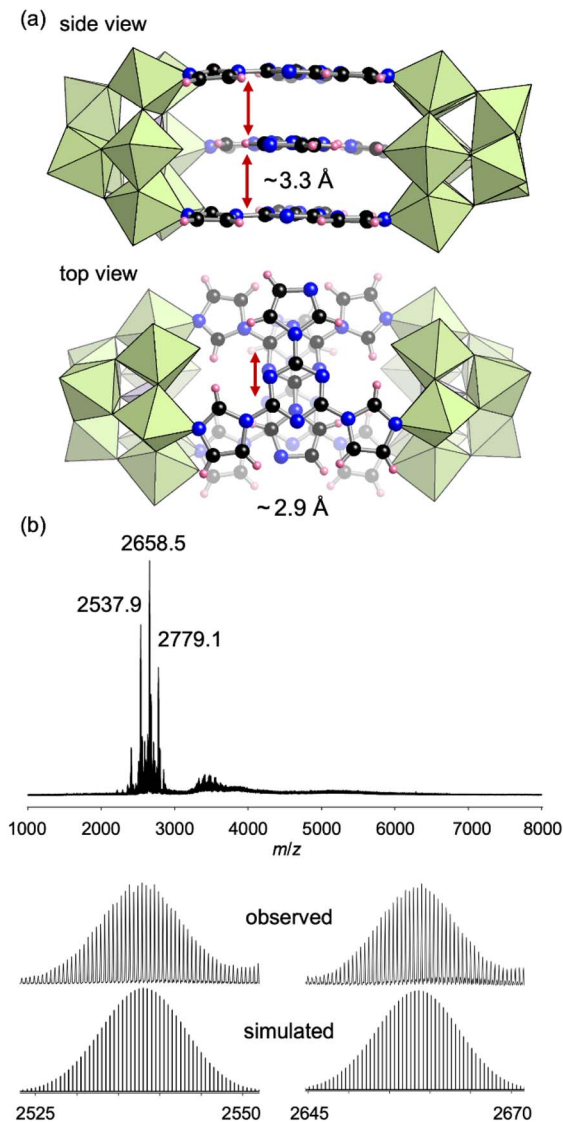


Fig. 5 (a) Crystal structure of the anion part of **III**. The distance between the **L3** ligand layers (side view,  $\sim 3.3$  Å) and the distance of the centers of the parallel ligands (top view,  $\sim 2.9$  Å) are shown. (b) ESI mass spectrum of **III** in acetonitrile. Inset: enlarged spectra and simulated patterns for  $m/z$  2537.9 ( $[\text{TBA}_6\text{H}(\text{PMo}_9\text{O}_{31})_2(\text{L3})_3(\text{CH}_3\text{CN})]^{2+}$ ) and 2658.5 ( $[\text{TBA}_7\text{H}(\text{PMo}_9\text{O}_{31})_2(\text{L3})_3]^{2+}$ ).

Despite three imidazole groups in **L3**, the obtained **III** was a dimer structure in which one of the three imidazole units remained uncoordinated in each ligand. The distance between the **L3** ligand layers in **III** was approximately 3.3 Å and the centers of the parallel ligands were split by approximately 2.9 Å (Fig. 5a), indicating the existence of  $[\pi-\sigma]^2$  interactions between the three **L3** ligands.<sup>12</sup> To avoid such interactions, we next used 1,3,5-tri(1*H*-imidazol-1-yl)benzene (**L4**), which possesses a benzene ring instead of a triazine at the center, as a ligand. Reacting **L4** with  $\text{TBA}_3[\text{PMo}_9\text{O}_{31}(\text{pyridine})_3]$  in 2 : 1 ratio in *N,N*-dimethylformamide at 50 °C afforded **IV** as a crude powder. Recrystallization of the crude product in a mixed solvent of *N,N*-dimethylacetamide and 1,4-dioxane afforded single crystals of

**IV**. X-ray crystallographic analysis revealed that the anion part of **IV** was a tetrahedral tetramer cage structure where four  $[\text{PMo}_9]$  units and four **L4** ligands were placed at the vertices and faces, respectively (Fig. 6a, Table S1†). The ESI mass spectrum of **IV** in  $\text{CH}_3\text{CN}$  exhibited signals at  $m/z$  2641.1, 2701.5, and 3440.7, which could be assigned to  $[\text{TBA}_{16}(\text{PMo}_9\text{O}_{31})_4(\text{L4})_4(\text{H}_2\text{O})]^{4+}$ ,  $[\text{TBA}_{17}(\text{PMo}_9\text{O}_{31})_4(\text{L4})_4(\text{OH})]^{4+}$ , and  $[\text{TBA}_{15}(\text{PMo}_9\text{O}_{31})_4(\text{L4})_4(\text{H}_2\text{O})]^{3+}$ , respectively (Fig. 6b).

The tetrahedral structure of **IV** had an inner cavity, where the distance between the P atom of the  $[\text{PMo}_9]$  unit and the center of the opposite ligand **L4** was about 12.9 Å (Fig. S6†). Some of the  $[\alpha\text{-PMo}_9]$  units were transformed into  $[\beta\text{-PMo}_9]$  units, and the X-ray crystallographic analysis was performed with 1 : 1 ratio of these units. Based on the above results as well as elemental analysis, TG-DTA, and  $^{31}\text{P}$  NMR spectra (Figs. S2d and S5b†), the formula of **IV** was determined to be  $\text{TBA}_{12}[(\text{PMo}_9\text{O}_{31})_4(\text{L4})_4](\text{C}_4\text{H}_9\text{NO})_4$ .

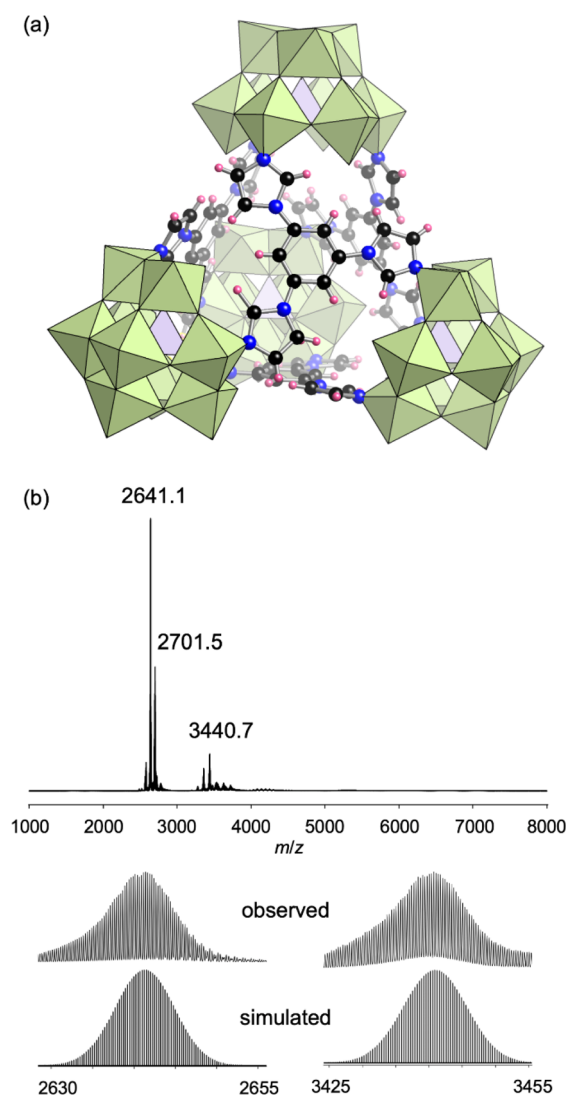


Fig. 6 (a) Crystal structure of the anion part of **IV**. (b) ESI mass spectrum of **IV** in acetonitrile. (Inset): enlarged spectrum and simulated pattern for  $m/z$  2641.1 ( $[\text{TBA}_{16}(\text{PMo}_9\text{O}_{31})_4(\text{L4})_4(\text{H}_2\text{O})]^{4+}$ ) and 3440.7 ( $[\text{TBA}_{15}(\text{PMo}_9\text{O}_{31})_4(\text{L4})_4(\text{H}_2\text{O})]^{3+}$ ).

## Conclusions

We report the first method for synthesizing self-assembled molecular hybrid structures *via* direct coordination of imidazole ligands to lacunary POMs. In particular, using the pyridine-coordinated trivacant lacunary polyoxomolybdate  $\text{TBA}_3[\text{A-}\alpha\text{-PMo}_9\text{O}_{31}(\text{pyridine})_3]$  as a precursor, we successfully synthesized several hybrids: the capped monomer **I**, pillar dimer **II**, sandwich-like dimer **III**, and tetrahedron tetramer **IV**. Because this synthesis method is applicable to various types of lacunary POMs and imidazole ligands, we expect it to help increase the number of POM–organic hybrids as well as their potential applications, such as in catalysis, photocatalysis, energy conversion, and sensors.

## Data availability

The data supporting this manuscript is available in the ESI† and available on request.

## Author contributions

H. S., A. J., C. L. performed the synthesis and characterizations. H. S., A. J., C. L., K. Yo. performed the crystallographic analysis. A. J. and K. S. performed the DFT calculations. All authors analyzed and discussed the results. K. S. conceived and directed the project. H. S., K. Yo., K. Ya., K. S. co-wrote the manuscript.

## Conflicts of interest

There are no conflicts of interest to declare.

## Acknowledgements

This study was supported in part by JST FOREST (JPMJFR213M), JSPS KAKENHI (22H04971), and the JSPS Core-to-Core program. Synchrotron X-ray diffraction measurements were conducted at SPring-8 with the approval of the Japan Synchrotron Radiation Research Institute (proposal numbers: 2023B1842, 2022B1605, 2022B1859). A part of computations was performed using Research Center for Computational Science, Okazaki, Japan (Project: 23-IMS-C106, 24-IMS-C101).

## Notes and references

- (a) S. R. Seidel and P. J. Stang, *Acc. Chem. Res.*, 2002, **35**, 972; (b) K. Harris, D. Fujita and M. Fujita, *Chem. Commun.*, 2013, **49**, 6703; (c) S. H. A. M. Leenders, R. Gramage-Doria, B. de Bruin and J. N. H. Reek, *Chem. Soc. Rev.*, 2015, **44**, 433; (d) Y. Fang, J. A. Powell, E. Li, Q. Wang, Z. Perry, A. Kirchon, X. Yang, Z. Xiao, C. Zhu, L. Zhang, F. Huang and H.-C. Zhou, *Chem. Soc. Rev.*, 2019, **48**, 4707; (e) X.-Z. Li, C.-B. Tian and Q.-F. Sun, *Chem. Rev.*, 2022, **122**, 6374; (f) H. Takezawa, K. Shitozawa and M. Fujita, *Nat. Chem.*, 2020, **12**, 574; (g) P. Mal, B. Breiner, K. Rissanen and J. R. Nitschke, *Science*, 2009, **324**, 1697.
- (a) M. T. Pope, *Heteropoly and Isopoly Oxometalates*, Springer, Berlin, 1983; (b) N. Mizuno and M. Misono, *Chem. Rev.*, 1998, **98**, 199; (c) C. L. Hill, in *Comprehensive Coordination Chemistry II*, ed. J. A. McCleverty and T. J. Meyer, Elsevier Pergamon, Amsterdam, 2003, vol. 4, p. 679; (d) H. N. Miras, J. Yan, D.-L. Long and L. Cronin, *Chem. Soc. Rev.*, 2012, **41**, 7403; (e) S.-S. Wang and G.-Y. Yang, *Chem. Rev.*, 2015, **115**, 4893; (f) N. I. Gumerova and A. Rompel, *Nat. Rev. Chem.*, 2018, **2**, 0112; (g) K. Suzuki, N. Mizuno and K. Yamaguchi, *ACS Catal.*, 2018, **8**, 10809; (h) A. Misra, K. Kozma, C. Streb and M. Nyman, *Angew. Chem., Int. Ed.*, 2020, **59**, 596.
- (a) A. Dolbecq, E. Dumas, C. R. Mayer and P. Mialane, *Chem. Rev.*, 2010, **110**, 6009; (b) J. M. Cameron, G. Guillemot, T. Galambos, S. S. Amin, E. Hampson, K. M. Haidaraly, G. N. Newton and G. Izzet, *Chem. Soc. Rev.*, 2022, **51**, 293; (c) F. Li and L. Xu, *Dalton Trans.*, 2011, **40**, 4024; (d) A. V. Anyushin, A. Kondinski and T. N. Parac-Vogt, *Chem. Soc. Rev.*, 2020, **49**, 382; (e) A. Proust, B. Matt, R. Villanneau, G. Guillemot, P. Gouzerh and G. Izzet, *Chem. Soc. Rev.*, 2012, **41**, 7605.
- (a) J. M. Breen and W. Schmitt, *Angew. Chem., Int. Ed.*, 2008, **47**, 6904; (b) M. B. Mahimaidoss, S. A. Krasnikov, L. Reck, C. I. Onet, J. M. Breen, N. Zhu, B. Marzec, I. V. Shvets and W. Schmitt, *Chem. Commun.*, 2014, 2265; (c) Z. Zhang, L. Wojtas and M. J. Zaworotko, *Chem. Sci.*, 2014, 927; (d) Y. Zhang, H. Gan, C. Qin, X. Wang, Z. Su and M. J. Zaworotko, *J. Am. Chem. Soc.*, 2018, 17365; (e) N. Xu, H. Gan, C. Qin, X. Wang and Z. Su, *Angew. Chem., Int. Ed.*, 2019, **58**, 4649; (f) Y. Gong, C. Qin, Y. Zhang, C. Sun, Q. Pan, X. Wang and Z. Su, *Angew. Chem., Int. Ed.*, 2020, **59**, 22034.
- (a) L.-L. Liu, L. Wang, X.-Y. Xiao, P. Yang, J. Zhao and U. Kortz, *Coord. Chem. Rev.*, 2024, **506**, 215687; (b) O. Oms, A. Dolbecq and P. Mialane, *Chem. Soc. Rev.*, 2012, **41**, 7497; (c) K. Suzuki, N. Mizuno and K. Yamaguchi, *J. Jpn. Petrol. Inst.*, 2020, **63**, 258.
- (a) G. S. Chorghade and M. T. Pope, *J. Am. Chem. Soc.*, 1987, **109**, 5134; (b) C. R. Mayer and R. Thouvenot, *J. Chem. Soc., Dalton Trans.*, 1998, 7; (c) S. Fujimoto, J. M. Cameron, R.-J. Wei, K. Kastner, D. Robinson, V. Sans, G. N. Newton and H. Oshio, *Inorg. Chem.*, 2017, **56**, 12169; (d) T. Minato, K. Suzuki, K. Yamaguchi and N. Mizuno, *Chem. - Eur. J.*, 2017, **23**, 14213; (e) A. Jimbo, C. Li, K. Yonesato, T. Ushiyama, K. Yamaguchi and K. Suzuki, *Chem. Sci.*, 2023, **14**, 10280.
- (a) S.-T. Zheng, J. Zhang, X.-X. Li, W.-H. Fang and G.-Y. Yang, *J. Am. Chem. Soc.*, 2010, **132**, 15102; (b) Q. Chang, X. Meng, W. Ruan, Y. Feng, R. Li, J. Zhu, Y. Ding, H. Lv, W. Wang, G. Chen and X. Fang, *Angew. Chem., Int. Ed.*, 2022, **61**, e202117637; (c) J. Guo, Q. Chang, Z. Liu, Y. Wang, C. Liu, M. Wang, D. Huang, G. Chen, H. Zhao, W. Wang and X. Fang, *Chem. Sci.*, 2021, **12**, 7361.
- (a) C. Li, N. Mizuno, K. Yamaguchi and K. Suzuki, *J. Am. Chem. Soc.*, 2019, **141**, 7687; (b) C. Li, K. Yamaguchi and K. Suzuki, *Angew. Chem., Int. Ed.*, 2021, **60**, 6960; (c) M. Yamaguchi, K. Shioya, C. Li, K. Yonesato, K. Murata,



- K. Ishii, K. Yamaguchi and K. Suzuki, *J. Am. Chem. Soc.*, 2024, **146**, 4549.
- 9 (a) A. Richaud, N. Barba-Behrens and F. Méndez, *Org. Lett.*, 2011, **13**, 972; (b) R. J. Sundberg and R. B. Martin, *Chem. Rev.*, 1974, **74**, 471.
- 10 (a) X.-W. Zhu, D. Luo, X.-P. Zhou and D. Li, *Coord. Chem. Rev.*, 2022, **455**, 214354; (b) P. Kukkar, K.-H. Kim, D. Kukkar and P. Singh, *Coord. Chem. Rev.*, 2021, **446**, 214109; (c) S.-S. Chen, *CrystEngComm*, 2016, **18**, 6543; (d) J.-P. Zhang, Y.-B. Zhang, J.-B. Lin and X.-M. Chen, *Chem. Rev.*, 2012, **112**, 1001; (e) J. R. Galán-Mascarós and K. R. Dunbar, *Angew. Chem., Int. Ed.*, 2003, **42**, 2289; (f) Q. Chen, Z. Chang, W.-C. Song, H. Song, H.-B. Song, T.-L. Hu and X.-H. Bu, *Angew. Chem., Int. Ed.*, 2013, **52**, 11550.
- 11 (a) H.-J. Pang, H.-Y. Ma, J. Peng, C.-J. Zhang, P.-P. Zhang and Z.-M. Su, *CrystEngComm*, 2011, **13**, 7079; (b) H. Zhao, L. Tao, F. Zhang, Y. Zhang, Y. Lui, H. Xu, G. Diao and L. Ni, *Chem. Commun.*, 2019, **55**, 1096; (c) X.-J. Yang, M. Sun, H.-Y. Zang, Y.-Y. Ma, X.-J. Feng, H.-Q. Tan, Y.-H. Wang and Y.-G. Li, *Chem.-Asian J.*, 2016, **11**, 858; (d) J. Du, J. Yu, J. Tang, J. Wang, W. Zhang, W. R. Thiel and M. Jia, *Eur. J. Inorg. Chem.*, 2011, **15**, 2361.
- 12 T. J. Mooibroek and P. Gamez, *Inorg. Chim. Acta*, 2007, **360**, 381.

